Chemo-mechanical modeling for prediction of alkali silica reaction (ASR) expansion

Stéphane Multon, Alain Sellier, Martin Cyr

Chemo-mechanical modeling for prediction of alkali silica reaction (ASR) expansion

Stéphane Multon [a*], Alain Sellier [a], Martin Cyr [a]

[(a)] *Université de Toulouse; UPS, INSA; LMDC (Laboratoire Matériaux et Durabilité des Constructions); 135, avenue de Rangueil; F-31 077 Toulouse Cedex 04, France*

Abstract

The effect of the size of the aggregate on ASR expansion has already been well illustrated. This paper presents a microscopic model to analyze the development of ASR expansion of mortars containing reactive aggregate of different sizes. The attack of the reactive silica by alkali was determined through the mass balance equation, which controls the diffusion mechanism in the aggregate and the fixation of the alkali in the ASR gels. The mechanical part of the model is based on the damage theory in order to assess the decrease of stiffness of the mortar due to cracking caused by ASR and to calculate the expansion of a Representative Elementary Volume (REV) of concrete. Parameters of the model were estimated by curve fitting the expansions of four experimental mortars. The paper shows that the decrease of expansion with the size of the aggregate and the increase of the expansion with the alkali content are reproduced by the model, which is able to predict the expansions of six other mortars containing two sizes of reactive aggregate and cast with two alkali contents.

Keywords: alkali-silica reaction (ASR), particle size, alkali content, expansion, model

[*] Corresponding author. *e-mail address:* multon@insa-toulouse.fr (Stéphane Multon)

1. Introduction

Alkali Silica Reaction is a chemical reaction between the alkalis of cement and the reactive silica of concrete structure aggregates. The reaction products are expansive gels which induce stresses, and hence cracking, in concrete. The main research on ASR concerns the expert appraisal of damaged structures [1-5]. Modeling ASR and the resulting expansion is necessary to obtain relevant predictions of the structural responses of damaged structures and models must take the chemical and physical aspects into account.

The LMDC (Laboratoire des Matériaux et Durabilité des Constructions), with EDF (Electricité de France) as a partner, has been working to establish a general method for the reassessment of ASR-damaged structures. The method uses expansion measurements on small specimens (2 x 2 x 16 cm) of mortar cast with crushed aggregates extracted from damaged structures [6-7] in order to evaluate the advancement of the reaction on the aggregates. As shown in [6-7], the advancement varies with the size of the aggregates because of the time taken for alkali to diffuse into the aggregate. One of the advantages of this method is that it performs calculations by using the state of advancement of the different aggregate sizes in the structure concrete, which allows relevant predictions to be obtained. However, this research needs to be completed by the development of microscopic modeling that uses the tests proposed in [6-7] in a reliable way, particularly according to the effect of the alkali content and the size of the reactive aggregate particles on the ASR-expansions. Predicting the expansion of concrete in real damaged structures is the final aim of this model. However, as a first step, it is used here to analyze laboratory experiments where the effects of mechanical stresses and environmental conditions on expansion are not considered. Similarly, alkali regeneration by calcium ions, which is a slow process [8-10], is not taken into account.

This paper deals with the development of an empirical microscopic ASR model. The main input data to such models are alkali and reactive silica contents, aggregate sizes, and mechanical properties of the mortar. The main result is the prediction of the ASR expansion of the concrete taking into consideration the physicochemical mechanisms of the reaction. Among the existing microscopic ASR models, some were developed to take the mechanics of ASR into consideration [11-12], and others focus on the chemical phenomena [13]. Finally, some models take both aspects into account [14-18]. Many phenomena of ASR can be described by the existing models (e.g. diffusion of alkali into the aggregates, gel permeation and imbibition); but others cannot be correctly represented yet (e.g. evolution of the concentration of alkali during the reaction, and expansion of concrete containing different sizes of reactive aggregate).

The microscopic model developed in this paper is based on some of these previous models [13-14, 17-18]. It can predict the damage and the expansion of a Representative Elementary Volume (REV) of concrete containing a mix of reactive aggregates of different sizes. The diffusion of alkali into the aggregate is taken into account; the production of the ASR gel increases with the molar concentration of alkalis in the aggregate. In the cement paste surrounding the reactive aggregate, the concentration of alkalis decreases with their diffusion towards the aggregate and their consumption by the ASR gel. The gel permeates into a part of the porous volume connected to the reactive aggregate. Once the available porous volume has been filled by the gel, the pressure due to ASR acts on the surrounding cement paste, leading to damage and expansion.

The modeling principles and assumptions are first presented and discussed. Then, the physicochemical and mechanical models are developed in two parts. Finally, the model is used to calculate the expansion of ten mortars containing different amounts of two sizes of reactive aggregate and having two alkali contents. Five parameters of the physicochemical

model cannot be obtained by direct measurements and are therefore calculated by inverse analysis using four of the ten mortars. The parameters thus obtained are used to predict the expansions of the other six mortars. Once the mechanical characteristics of the sound concrete are known, no additional fitting of parameters is necessary for the mechanical modeling. The last part points out the qualities and the limitations of the model and gives some indications as to how it could be improved.

2. Principles

2.1 Physicochemistry and mechanics of ASR

As in previous works [13,15,18], the model developed in this paper used the reaction mechanisms presented by Dent Glasser and Kataoka [19]:

- The first part of the reaction is the diffusion of the alkali and hydroxyl ions into the reactive aggregate, and the destruction of the silanol and siloxane bonds contained in the reactive silica.

- The second part is the formation of the ASR gels in presence of water and calcium ions [19-21]. Once formed, the gel permeates through a part of the connected porous volume between aggregate and cement paste and fills a part of the connected porosity [22]. Then the gel exerts a pressure on the cement paste, which causes cracking and expansion of the concrete.

Moreover, in order to complete the physical considerations, assumptions based on numerous experimentations already published were made: the existence of a threshold in alkali concentration under which ASR does not occur [23-26], the high nonlinearity of the dissolution of the reactive silica with pH [29] and the stœchiometry of ASR gels [30-32].

2.2 Assumptions

It is not possible to consider all the physical and chemical mechanisms of such a reaction occurring in a complex medium like concrete. Simplifications have to be assumed in order to model ASR expansion in accordance with most phenomena.

2.2.1 Geometry

The reactive aggregate and the Relative Elementary Volume (REV) of concrete surrounding the reactive aggregate are assumed to be spherical (Figure 1).

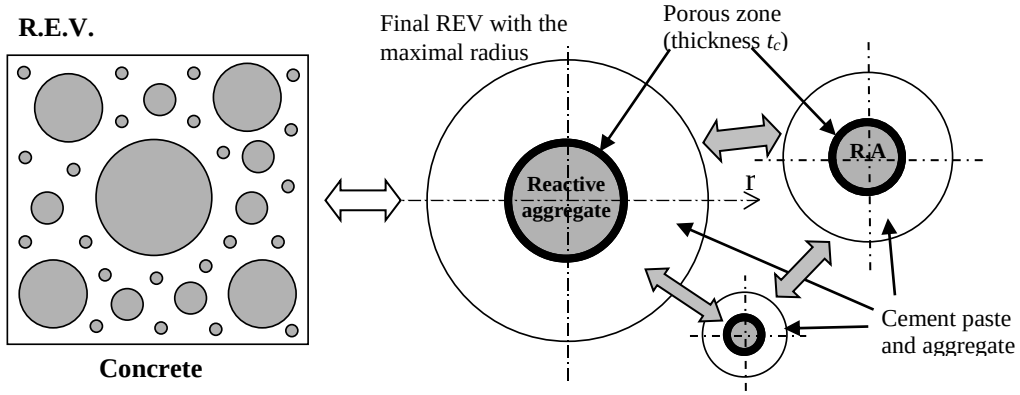

Figure 1 – Definition of the Relative Elementary Volume for several reactive aggregate sizes [18]

The radius of the REV depends on the radius and the content of the reactive aggregate in concrete, as given by equation 1 [18]:

$$R_{REV}^{a} = \frac{R_a}{\sqrt[3]{\phi_a . C_{agg}}} \quad (1)$$

with:

a, a superscript relative to the size fraction of the reactive aggregate with mean radius R_a

R^a_{REV} the REV radius corresponding to the aggregate size fraction *a*

ϕ_a the volume fraction of reactive aggregates with mean radius R_a

C_{agg} the volume fraction of all the aggregate per m^3 of concrete.

The number of reactive aggregates per m^3 of concrete N_a is equal to:

$$N_a = \frac{\phi_a . C_{agg}}{\frac{4}{3}\pi R_a^3} \quad (2)$$

2.2.2 Diffusion of alkali and attack of reactive silica

In the model presented in [18], the diffusion of the ionic species into both reactive aggregate and cement paste surrounding the aggregate is considered. However, at each time step, the concentrations of ionic species are roughly homogeneous in the cement paste. This can be explained by the differences between the coefficients of diffusion in the cement paste (about 10^{-11} m^2/s) and in the aggregate (about 10^{-15} m^2/s). Thus, diffusion into the cement paste appears to be instantaneous compared to diffusion into the aggregate, so the alkali concentration was assumed to be uniform in the paste in the present model. This constitutes the main simplification in relation to Poyet's modeling [18].

Moreover, the aggregate was taken as spherical. Thus the concentrations of the ionic species diffusing into the aggregate depend only on the time and on the radius *r* from the centre of the reactive aggregate (Figure 2).

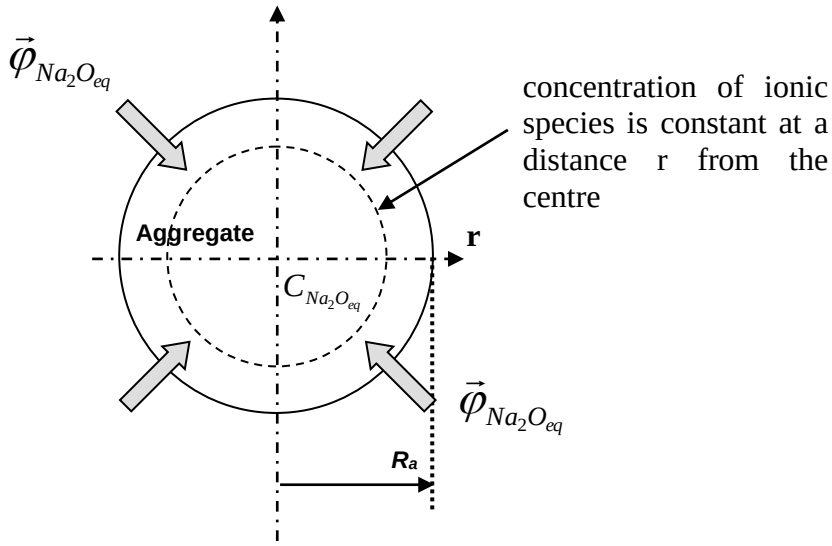

Figure 2 – Diffusion of Na_2O_{eq} in aggregate

Several authors showed that no expansion occurred in concrete containing alkali silica reactive aggregate for low alkali contents: under a threshold lying between 3 and 5 kg/m^3 [23-26] or for an alkali concentration lower than 0.5 or 0.6 mol/l of Na^+ [27-28].Urhan reports that the solubility of silica is quite constant in a solution having a pH of less than 9 or 10 but increases rapidly for higher pH [29]. Due to the high nonlinearity between the pH and the solubility of the silica and to the relationship between the value of the pH in a solution and the concentration of alkali, the destruction of the reactive silica was assumed to increase significantly when the concentration of alkalis in a part of the aggregate was higher than a threshold concentration noted Na_{th}. When the threshold is reached and passed, the present model assumes that gel formation increases with a rate proportional to the difference between the alkali concentration in the aggregate and the threshold. The same rate is taken for the alkali consumption by the ASR gels. Therefore, the kinetics of the reaction, and thus of the gel formation, is assumed to be controlled by the destruction of the reactive silica due to alkali diffusion. Some authors [8-10] consider that the gel formation depends on the presence of calcium ions. This has not been taken into account in the model. However, as calcium is provided by portlandite dissolution and as this dissolution is not possible while the alkali content is high, the need for calcium can be neglected during the first step of an accelerated test. This aspect of the reaction will have to be carefully considered for the simulation of long-term ASR phenomena. So the extension of the present model to structural applications will have to include calcium substitution.

2.2.3 ASR gel

Another problem for ASR modeling concerns the assumptions on the compositions of the gels produced by the reaction. The compositions of the gels depend on many parameters, such as gel position in the concrete (in or out of the aggregate) and its age (it is usually assumed that old gels contain more calcium than new). The Na_2O / SiO_2 ratio in the gels varies from about

0.1 to 0.4 [30-32]. It is quite difficult to obtain a relevant and representative value for the gel composition. In the model presented here, the Na_2O / SiO_2 ratio is assumed to be equal to the mean value 0.2 obtained in laboratory experiments in [32]; it is assumed that 1 mole of Na_2O_{eq} reacts with 5 moles of SiO_2 to give 1 mole of ASR gel. The volume of gel produced by one size of aggregate n_g^a is obtained by multiplying the number of moles of ASR gel produced by the aggregate *a* by the molar volume of the gel V_{gel}^{mol} (in m^3/mol). The total volume of gel formed is then the sum of the volume of gel produced by all the aggregates (in m^3):

$$V_g = \sum_i n_g^a \times V_{gel}^{mol} \quad (3)$$

As described just above, after its formation, the gel can permeate through a part of the connected porous volume surrounding the aggregate [33] or can stay in the cracks of the aggregate. This part of connected porosity is modeled as a volume of porosity totally filled by the gel with an equivalent thickness t_c (Figure 1, Eq 4). The equivalent thickness is assumed not to change with the size of the aggregate. Thus, the volume of gel necessary to fill this porosity, which consequently which does not exert pressure, is equal to the connected porosity (p):

$$V_{por} = \frac{4}{3}\pi\left(\left(R_a + t_c\right)^3 - R_a^3\right)p \quad (4)$$

The larger the aggregate size, the lower the ratio ‘connected porous volume / aggregate volume’. Therefore the largest aggregate causes the largest ASR-expansion.

2.2.4 Mechanical considerations

The model is supposed to calculate ASR expansion for stress free specimens. Moreover, the mechanical properties are taken to be isotropic and, thus, the mechanical behavior of the aggregate and of the cement paste in the REV is taken as isotropic. The behaviors of the two media are assumed to be elastic for stresses lower than their compressive and tensile strengths. The expansions due to ASR occur over long periods. During the process, the materials are not subjected to instantaneous loading but to progressive stresses which cause creep strains in the concrete [5]. In order to take the effect of concrete creep on the ASR expansion into account, the calculations are performed with a long-term Young's modulus equal to a third of the instantaneous Young's modulus (which is the usual value used in the French reinforced concrete design code [34]). For the same stress, using the long-term modulus rather than the instantaneous modulus leads to larger strains. The strains are then equal to the sum of the instantaneous strains due to the ASR gel pressure and the creep strains of the cement paste under the ASR gel pressure. If the stresses become higher than the tensile strengths of the materials, cracking and damage occur in the concrete. In the following calculations, the crack density is consistent with the damage to the concrete calculated by the model (the damage is defined as the decrease of the long-term Young's modulus due to cracking). After cracking, the gel is assumed to permeate into the cracks.

3. Physicochemical modeling

The physicochemical modeling concerns the diffusion of the alkali ions into the aggregate and the formation of the ASR gel. The alkali diffusion into the aggregate is controlled by the mass balance equation with a depletion term to represent the consumption of alkali during the formation of the ASR gel. The volume of gel produced by the reaction can then be calculated from the alkali consumed in the mass balance equation. The equations are solved numerically by using a geometrical discretization based on finite volumes and time discretization by Euler's method.

3.1 Mass balance equation

3.1.1 Alkali diffusion in aggregate

Just after casting, the alkali concentration is high in the cement paste and negligible in the aggregate. Therefore, a flux of alkali (Na^+ and K^+) appears between the cement paste and the core of the aggregate. The mass balance of alkali in the aggregate with the assumed spherical symmetry can be described by the equation:

$$\frac{\partial}{\partial t}\left(p_{agg} S_r C_{Na}\right) = \frac{1}{r^2}\frac{\partial}{\partial r}\left(D.r^2 \frac{dC_{Na}}{dr}\right) + S\left(C_{Na}\right) \quad (5)$$

with:

t the time

p_{agg} the porosity of the aggregate,

S_r the saturation degree,

C_{Na} the concentration of alkali (Na^+ and K^+),

r the distance from the center of the aggregate,

D coefficient of diffusion of alkalis into the aggregate,

and $S(C_{Na})$ the depletion term that represents alkali consumption.

In order to solve the equation, two boundary conditions were used:

- at the centre of the aggregate ($r=0$), the flux is equal to zero;
- at the external boundary ($r=R_a$), the alkali concentration is equal to C_{Na}^{cp}, the alkali concentration in the cement paste. For the initial condition, this concentration is equal to:

$$C_{Na}^{cp} = 2 \times \frac{M_{Na2O}}{M_{Na2O}^{mol}} \times \frac{1}{p_{cp} S_r \left(1 - C_{agg}\right)} \text{ with } p_{cp} = \frac{p_{mort} - p_{agg}.C_{agg}}{\left(1 - C_{agg}\right)} \quad (6) \quad (7)$$

with:

M_{Na2O} the mass of equivalent alkali per m^3 of concrete,

M^{mol}_{Na2O} the molar mass of equivalent alkali (equal to 0.062 kg/mol),

p_{cp}, p_{mor}, p_{agg} the porosity of the cement paste, mortar, and aggregate respectively,

and C_{agg} the aggregate concentration per m^3 of concrete.

During the process, the concentration of alkali in the cement paste decreases due to alkali diffusion into the aggregate (see next part).

3.1.2 Alkali concentration in the cement paste

The variation of alkali content in the cement paste is due to the diffusion from the paste to the aggregate. It is equal to the sum of the flux of alkali at the boundary ($r=R_a$) between all the aggregate and the paste. For concrete containing several size fractions, a, of reactive aggregate, the flux has to be summed over all of them. It can be calculated by:

$$\frac{\partial}{\partial t}\left(p_{cp} S_r C_{Na}\right) = \sum_a N_a.D.4\pi R_a^2 \frac{dC_{Na}^a}{dr}\left(R_a\right) \quad (8)$$

with N_a the number of reactive aggregates (Eq 2).

3.1.3 Consumption of alkalis

As explained in the ‘Assumptions’ section, the consumption kinetics of alkalis is assumed to be proportional to the difference between the concentration of alkali in the aggregate and the

threshold above which the silica dissolution starts. Thus, the depletion term of the mass balance equation is:

$$S(C_{Na}) = f\langle C_{Na} - Na_{thr}\rangle^{+} \quad (9)$$

With: *f*, the alkali fixation coefficient. This is the coefficient of proportionality between the consumption kinetics of alkali and the difference between the concentration of alkali in the aggregate and the alkali threshold. *f* is a negative parameter. Note that it could depend on the temperature if AAR dependence on temperature is to be modeled.

$\langle X\rangle^{+}$ is equal to X if $X > 0$ or equal to 0 if $X \leq 0$.

$S(C_{Na2O})$ is the amount of alkali fixed per m^3 of aggregate. If the concentration of alkalis in the aggregate is lower than the alkali threshold, the term is zero; there is no consumption of alkali and no ASR-gel formation. If the concentration is higher than the threshold, the consumption of alkali starts with the kinetics given by equation 9.

Moreover, the consumption of alkali has to be stopped when all the reactive silica contained in the aggregate has reacted with alkali. As the Na_2O / SiO_2 ratio of the gel is assumed to be equal to 0.2 [32], the end of the alkali fixation is obtained when the amount of alkali fixed by the aggregate is equal to 0.2 times the reactive silica content of the aggregate.

Note: The unit of the alkali fixation coefficient is (mol/m^3 of aggregate) per (mol/m^3 of solution) per second.

3.2 Formation of the ASR gel

The number of moles of ASR gel produced in the aggregate *a* at time step *t* is equal to the number of moles of Na_2O consumed by the reaction, thus half the number of moles of Na^+:

$$n_g^a = \frac{4}{3}\pi R_a^3 \times \int_0^t \frac{S(C_{Na})}{2}\,dt \quad (10)$$

Finally, the volume of gel produced by the reaction is given by the Equation 3.

4. Mechanical modeling

The main result of the chemical modeling is V_g, the volume of ASR gel formed by the reaction. The volume of gel is then used to determine the strain induced on the REV and finally the expansion of the damaged concrete caused by the chemical reaction. As for the chemical modeling, the equations of mechanical equilibrium are calculated on the spherical REV, as has already been described for elastic conditions in [11,14,17]. In the REV, the mechanical equations are used for two media: *a*, the aggregate under study, and *SC*, the concrete surrounding the studied aggregate (medium including cement paste and other aggregate – Figure 3). The cracking due to ASR is taken into account by isotropic mechanical damage [35-36]. Thus, the mechanical problem is assumed to be non-linear elastic due to the introduction of the damage variable. The equations developed below present an analytical solution and are applied to each aggregate size.

4.1 Strain-stress equations

The ASR gel is supposed to be incompressible compared to the elastic properties of the cement paste and aggregate. Therefore, the ASR expansion can be taken into account as an imposed strain in the aggregate elastic constitutive law:

$$\underline{\underline{\sigma_a}} = \lambda_a tr\,\underline{\underline{\varepsilon_a}}.\underline{\underline{I}} + 2.\mu_a.\underline{\underline{\varepsilon_a}} - (3\lambda_a + 2\mu_a).\underline{\underline{\varepsilon_{imp1}}}(t) \quad (11)$$

The constitutive law of the medium *SC* only considers the elastic effect of the material:

$$\underline{\underline{\sigma_{SC}}} = \lambda_{SC} tr\,\underline{\underline{\varepsilon_{SC}}}.\underline{\underline{I}} + 2.\mu_{SC}.\underline{\underline{\varepsilon_{SC}}} \quad (12)$$

with

$\underline{\underline{\sigma}}$ the stress matrix for each material,

$\underline{\underline{\varepsilon}}$ the strain matrix for each material,

$\underline{\underline{I}}$ the unit matrix,

274 λ and μ are, for each material:

$$\lambda = \frac{E\nu}{(1+\nu)(1-2\nu)} \text{ and } \mu = \frac{E}{2.(1+\nu)} \quad (13)$$

(14)

275 where E is the Young's modulus and ν, the Poisson's coefficient of the medium.

276 ε_{imp1} is the imposed strain applied to the aggregate.

277 The imposed strain applied to the aggregate is isotropic. It is assessed from the increase in
278 volume due to gel formation; the details of the calculation are given below (Equation 23).

279 The displacements in the materials are deduced by solving the equilibrium equation of the
280 elastic solids $\underline{div}\,\underline{\underline{\sigma}} = 0$ assuming spherical symmetry. Displacements u_a in the aggregate and
281 u_{SC} in the surrounding concrete then depend only on the radius r:

In the aggregate *a*: $$\underline{u_a}(r) = A_a.r.\underline{e_r} \quad (15)$$

In the surrounding concrete *SC*: $$\underline{u_{SC}}(r) = \left(A_{SC}.r + \frac{B_{SC}}{r^2}\right).\underline{e_r} \quad (16)$$

282 The three unknown constants (A_a, A_{SC} and B_{SC}) are determined from the following
283 boundary conditions (Figure 3):

284 - The radial displacements at the boundary between the aggregate and the surrounding
285 concrete are equal;
286 - The radial stresses are continuous at the boundary between the aggregate and the
287 surrounding concrete;
288 - The radial stress on the external surface is equal to zero (unloaded REV) (note: this
289 assumption leads to a free swelling model).

290 The mechanical equations can thus be solved and the variation of the stresses in the two
291 media can be analyzed. Due to the gel swelling, the aggregate is subjected to an isotropic
292 stress (pressure). This pressure is balanced by radial compressive stress in the concrete

surrounding the aggregate (decreasing from the aggregate pressure (at R_a) to zero on the REV external surface), and tensile stress in the tangential directions. The variation of the tensile stress in the tangential directions $\sigma_{\theta\theta}$ and $\sigma_{\varphi\varphi}$ with the radius has been plotted in Figure 3.

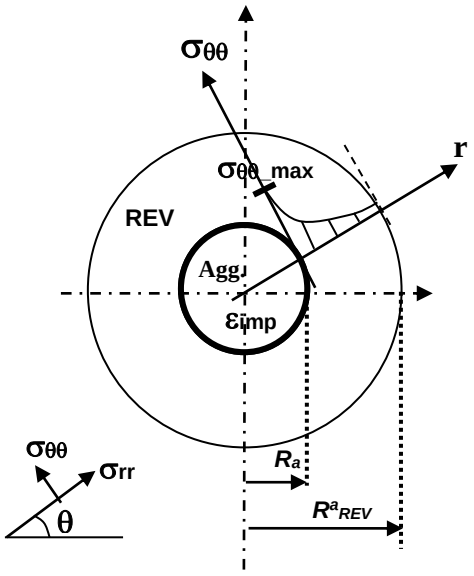

Figure 3 – Tensile stress in the REV subjected to ASR induced strains

The maximum tensile stress is located at the boundary between the aggregate and the surrounding concrete. As the strength of concrete is higher in compression (f_c) than in tension (f_t,), radial cracks due to the tensile stresses appear first and damage the surrounding concrete zone between the aggregate (R_a) and a radius R_d ($R_d - R_a$ corresponds to the crack length). In the following section, the damage theory is used to replace the cracked concrete by an equivalent concrete with a reduced Young's modulus. This modeling has the advantage of leading to an equivalent elastic problem, governed by the same set of equations as the previous ones, but with a lower Young's modulus.

4.2 Damaged REV

4.2.1 Damaged Young's modulus of the REV

The REV contains several reactive aggregates (Figure 1), which all cause cracks in the REV. The interactions between the cracks of the different aggregates in the REV cause a decrease in the concrete modulus. This can be modeled by a damage variable [35]. The damage evaluation method is based on the strain equivalence principle [36]: the cracked medium (initial Young's modulus E_0) is replaced by an equivalent medium without cracks but with a lower modulus E_d (Figure 4) leading to the same displacement as the cracked one with the initial Young's modulus.

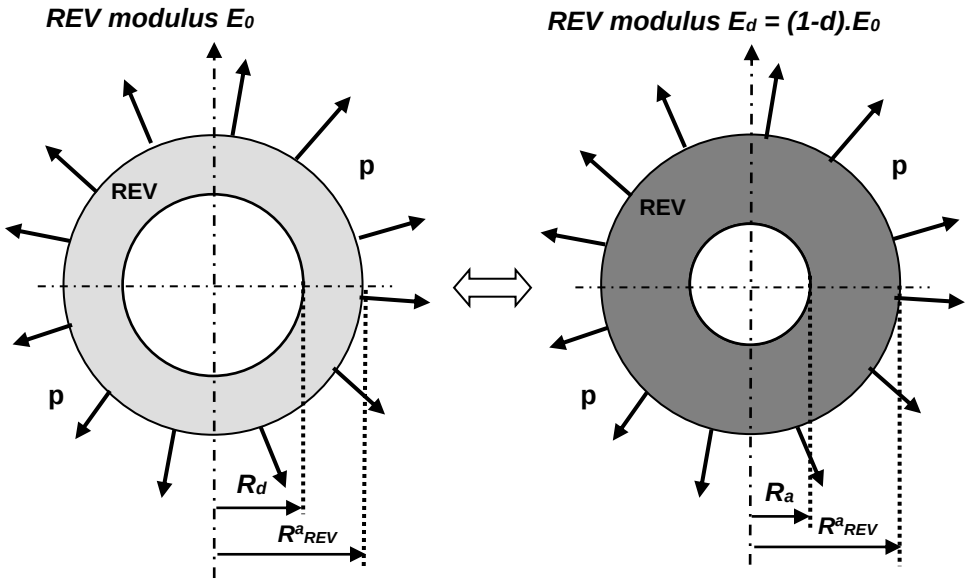

Figure 4 – Determination of the modulus of the damaged concrete

Therefore, as the cracked zone cannot withstand radial tension exceeding the tensile strength, the residual uncracked surrounding concrete is equivalent to a hollow sphere with inner and outer radii equal to R_d and R^a_{REV} under pressure p. According to the strain equivalence principle, the radial strain of this hollow sphere must be equal to the radial strain of the

uncracked hollow sphere with inner and outer radii equal to R_a and R^a_{REV} under pressure p but with a damaged Young modulus E_d (Figure 4). The damaged variable is then defined by:

$$d = 1 - \frac{E_d}{E_0} \tag{17}$$

Thus, the first hollow sphere, with a modulus of E_0, and the second one, with a modulus of $(1-d)E_0$ (Figure 4), have the same stiffness. If the inner radius R_d of the first sphere is equal to R_a, the strain of the cracked medium is equal to the strain of the medium without cracks and the damage d is equal to 0. If the inner radius R_d of the first sphere becomes close to the outer radius R^a_{REV}, the strain of the cracked medium increases and the damage d increases towards 1. Calculations are successively performed for all the aggregate size fractions a, and the maximum value of damage is used to determine the modulus of the equivalent medium E_d:

$$E_d = (1-d)E_0 \tag{18}$$

4.2.2 Evaluation of the REV expansion

Finally, the mechanical problem studied to assess the ASR-expansion is presented in Figure 5. As explained above, the model assumes that the cracks close to the aggregate are filled by the ASR gels. Thus, three parts can be distinguished (Figure 5): the central aggregate (between radii *0* and R_a), the cracked zone filled by the gel (between radii R_a and R_{cz}) and the part of the REV not yet cracked.

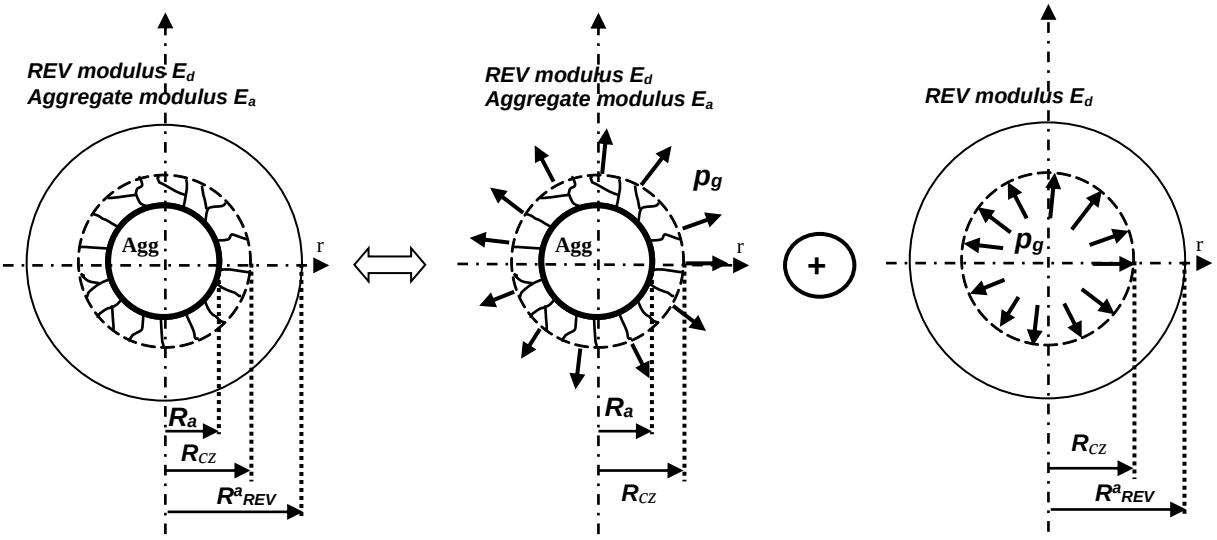

Figure 5 – Mechanical equilibrium of the damaged REV

As the gel reaches the cracks connected to the reactive aggregate, the radius R_{cz} corresponds to the radius R_d used to determine the damage (Figure 4). The gel pressure is constant in both the aggregate and the cracked zone; it is then applied to the internal boundary of the surrounding uncracked concrete. The modulus of the whole medium surrounding the aggregate is equal to E_d according to the damaged Young's modulus evaluated just above. The following behavior equation, concerning the part of the REV surrounding the aggregate and filled by the ASR gel, had to be added:

- the constitutive law:

$$\underline{\underline{\sigma_{cz}}} = \lambda_{fg} tr\,\underline{\underline{\varepsilon_{cz}}}.\underline{\underline{I}} + 2.\mu_{cz}.\underline{\underline{\varepsilon_{cz}}} - (3\lambda_{cz} + 2\mu_{cz}).\underline{\underline{\varepsilon_{imp2}(t)}} \tag{19}$$

where

ε_{imp2} is the imposed strain applied to the cracked zone of the surrounding concrete due to presence of ASR gel in the cracks;

the displacement is

$$\underline{u_{cz}}(r) = \left(A_{cz}.r + \frac{B_{cz}}{r^2} \right).\underline{e_r} \tag{20}$$

The two supplementary unknown constants A_{cz} and B_{cz} can be determined from two supplementary boundary conditions: the continuity of radial displacements and radial stresses at the boundary between the cracked zone and the surrounding concrete. The mechanical equations can thus be solved in function of R_{cz}, ε_{imp1} and ε_{imp2}. Three last equations are needed to assess the three unknown values of R_{cz}, ε_{imp1} and ε_{imp2}. The tensile stress $\sigma_{\theta\theta}$ is equal to the concrete tensile strength f_t for the radius R_{cz}:

$$\sigma_{\theta\theta}^{SC}(R_{cz}) = f_t \tag{21}$$

The effect of the imposed deformations ε_{imp1} and ε_{imp2} in the aggregate and in the concrete filled by the gel can be compared to a pressure p_g in both the aggregate and the cracked zone (Figure 5). As the pressure p_g is an isotropic stress, in the cracked zone filled by the gel

$$\sigma_{rr}^{cz}(R_{cz}) = \sigma_{\theta\theta}^{cz}(R_{cz}) \tag{22}$$

The imposed strains applied to the aggregate and to the cracked zone are the relative increase in the volume due to the production of gel by ASR. However, as explained above, a part of the gel fills the porous volume surrounding the aggregate (determined by equation 3) and does not participate in the expansion. The imposed strain is then equal to the volume of gel V_g minus the connected porosity V_{por} filled by the gel compared to the volume of the aggregate. Thus, the last equation is given by chemical modeling:

$$\left\langle V_g - V_{por} \right\rangle^+ = \frac{4}{3}\pi R_a^3 \varepsilon_{imp1} + \frac{4}{3}\pi\left(R_{cz}^3 - R_a^3\right)\varepsilon_{imp2} \tag{23}$$

where $\left\langle X \right\rangle^+$ is equal to X if $X > 0$ or equal to 0 if $X \leq 0$.

The damage to the concrete is obtained by substituting the volume of gel determined by the chemical modeling (Eq. 3) in Eq 23. The expansion induced by ASR in each aggregate size fraction can thus be calculated. For the aggregate size fraction a:

$$\varepsilon_a = \frac{u_{rr}\left(R^a_{REV}\right)}{R^a_{REV}} \tag{24}$$

with R^a_{REV} the radius of the REV corresponding to the aggregate size fraction *i*.

If the concrete contains several aggregate size fractions, the resulting strain is assumed to be the sum of expansions induced by each fraction:

$$\varepsilon_{ASR} = \sum_a \varepsilon_a \tag{25}$$

The relationship between the damage and the expansion of one reactive aggregate obtained by this model has been plotted in Figure 6. It is interesting to compare these values to experimental data but only a few papers deal with the decrease of direct tensile strength with ASR expansion, and none with the decrease of the tensile modulus. Siemes and Visser measured a decrease greater than 85% in the direct tensile strength for expansions between 0.05% and 0.1% [37]. For the same ASR expansions (between 0.05 and 0.1%), the damage calculated by the model is between 60 and 75%, which is slightly lower than the experimental values.

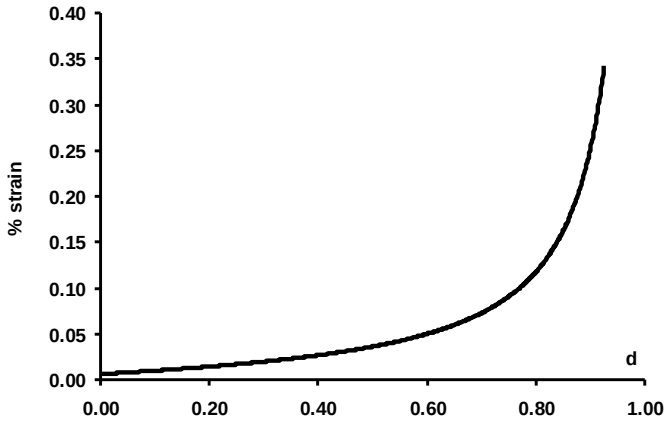

Figure 6 – Relationship between the damage (d) and the expansion of the REV

The mechanical modeling uses only five parameters: the Young's modulus and the Poisson's coefficient of the aggregate and mortar (E_a, ν_a and E_m, ν_m) and the tensile strength of the mortar f_t; no other fitting is necessary.

5. Comparison with experiments

The last part of the paper shows some calculations performed with the model developed in the previous parts. In order to assess the capability of the model to represent and predict real ASR expansions, the analysis is divided into three parts. First, experiments used to fit and test the model are presented. Then, the identification of the parameters is carried out and discussed. For the identification, the measurements of expansion performed on four different mortars were used. Finally, the model is used to calculate the expansion of six other mortars. The calculated expansions are compared to the measured ones and the differences are discussed.

5.1 Experiments

The experiments used to check the capability of the model to predict ASR expansion have been presented and analyzed in a previous paper [38]. Therefore, only the parameters used by the model are dealt with here. Expansion was measured on mortar prisms with a water-cement ratio of 0.5. The sand and cement contents were 1613.4 kg/m3 and 537.8 kg/m3 respectively. Two distinct Na/Si ratios were studied by adjusting the alkali contents (Na_2O_{eq}) to 6.2 and 13.4 kg of alkali per m^3 of mortar (addition of NaOH in the mixing water). Three size fractions of aggregate were used: FS for small aggregates (80–160 μm), FM for medium aggregates (315–630 μm) and FL for large ones (1.25–3.15 mm). The reactive aggregate was a siliceous limestone. In the experimental study, only fractions FS and FL were composed of reactive aggregates, the medium size aggregates were not reactive but were introduced into the formulation to obtain an acceptable particle size distribution. The reactive silica contents of the two reactive fractions were measured through a chemical analysis based on basic attack [38]; the reactive SiO_2 contents were equal to 9.4% and 12.4% per kg of aggregate for FS and FL. The particle size distribution was the same for all the mortars: 30% of FS, 40% of FM and 30% of FL. Different proportions of reactive and non-reactive aggregates from the two size

fractions FS and FL were used to make 5 reactive mortars for each alkali content, with always 30% of reactive particles (Figure 7).

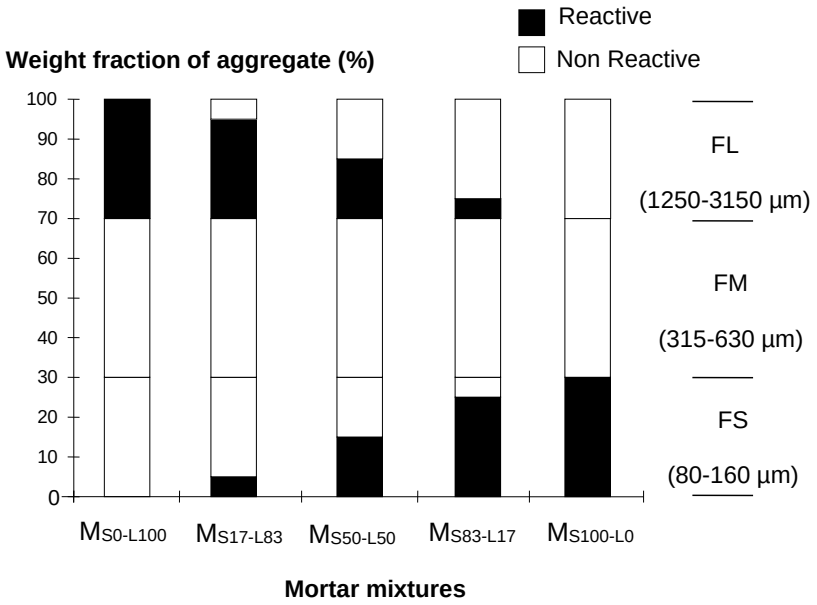

Figure 7 – Particle size distribution of the five mortars (in black: reactive aggregate, in white: non-reactive aggregate)

The mortar $M_{S0\text{-}L100}$ contained 0% of reactive particles in the SL fraction while 100% of the particles of the FL fraction were reactive. For the mortar $M_{S100\text{-}L0}$, 100% of the smallest reactive particles (FS) were reactive and all the other particles were non-reactive. The reactive particle contents of the mortars $M_{S17\text{-}L83}$, $M_{S50\text{-}L50}$ and $M_{S83\text{-}L17}$, lay between these two values. The ASR expansions presented in Figures 8 and 9, and used for the identification of the parameters and for the analysis of the model were obtained by subtracting the expansion of the reference mortar (without reactive aggregate) from the total expansion [38]. Thus, the strains were only caused by the pressure of the ASR gel and not by the pressure due to water absorption. The water porosity of each of the mortars was measured at the end of the experiment (Table 1), using AFPC-AFREM method [39]. Values were between 17 and 20%.

Table 1 – Porosity of the mortars in %

Alkali content of the mix design	$M_{S0\text{-}L100}$	$M_{S17\text{-}L83}$	$M_{S50\text{-}L50}$	$M_{S83\text{-}L17}$	$M_{S100\text{-}L0}$
6.2 kg / m^3	17.5	16.9	17.3	17.6	17.6
13.4 kg / m^3	20	19.9	19.6	18.9	17.9

5.2 Assessment of the parameters

Table 2 sums up the various parameters of the two models, with the symbols, the method used for identification, the values and the units. The following parts explain how the values were obtained.

Table 2 – Parameter identification

Parameter	Symbol	Identification	Value	Units
Physicochemical modeling				
Aggregate				
Coefficient of diffusion	D	curve fitting	3.5×10^{-13}	m²/s
Porosity	p	usual value	0.01	%
Paste				
Porosity of mortar	p_{mort}	measurement	17.-20.	%
Thickness of the connected porous interface zone	t_c	curve fitting	0.63×10^{-6}	m
Gel				
Molar volume of ASR gel	V_{gel}^{mol}	curve fitting	18.2×10^{-6}	m^3/mol
Alkali threshold	Na_{th}	curve fitting	620.	mol/m^3
alkali fixation coefficient	f	curve fitting	$- 6.5 \times 10^{-7}$	$m^3/m^3/s$
Mechanical modeling				
Aggregate				
Young's modulus	E_a	usual value	70000.	MPa
Poisson's coefficient	ν_a	usual value	0.2	-
Mortar				
Young's modulus	E_{REV}	usual value	9000.	MPa
Poisson's coefficient	ν_{REV}	usual value	0.2	-
Tensile strength	f_t	usual value	3.	MPa

5.2.1 Parameters of the physicochemical modeling

The first parameters needed for the physicochemical modeling are given by the mix-design information (see above: size and volume fractions of particles, alkali and reactive silica contents). Taking all the information into account, the aggregate concentration per m^3 of concrete C_{agg} could be calculated: it was equal to 0.61.

The porosity of the aggregate was taken as the value of 0.01% given by a previous work [40]. The porosity of the cement paste was calculated with equation 7. The last five parameters (coefficient of diffusion, thickness of the connected porous interface zone, molar volume of

ASR gel, threshold concentration Na_{th} and alkali fixation coefficient) of the physicochemical modeling were obtained by curve fitting on four mortars of the experimental study as explained in 5.2.3.

5.2.2 Parameters of the mechanical modeling

All the parameters of the mechanical modeling (Table 2) were obtained from the literature. The Young's modulus of the siliceous limestone was determined in a previous experiment [41]. The instantaneous Young's modulus of the mortar was taken as equal to a frequently found value for a mortar with a ratio W/C of 0.5: about 27000 MPa. As explained in the presentation of the assumptions, a long-term Young's modulus equal to one third of the instantaneous Young's modulus was used in the calculations in order to take the creep effect into account. The Poisson's coefficients of aggregate and mortar were taken as 0.2. The tensile strength of the mortar was estimated at 3 MPa. None of the parameters of the mechanical modeling were fitted.

5.2.3 Identification by curve fitting

The five parameters (coefficient of diffusion, thickness of the connected porous interface zone, molar volume of ASR gel, threshold concentration Na_{th} and alkali fixation coefficient) were obtained by curve fitting the expansions of four mortars of the experimental study: the last expansion measured on $M_{S0\text{-}L100}$ with 6.2 kg/m^3 of alkali and M2, $M_{S100\text{-}L0}$ with 13.4 kg/m^3 of alkali, and the whole expansion curves of $M_{S50\text{-}L50}$ with 6.2 kg/m^3 of alkali and $M_{S17\text{-}L83}$ with 13.4 kg/m^3 of alkali (Figure 8). First, the molar volume of ASR gel and the thickness of the connected porous zone were determined to fit the last expansion measured on the mortars $M_{S0\text{-}L100}$ - 6.2 kg/m^3, $M_{S17\text{-}L83}$ and $M_{S100\text{-}L0}$ - 13.4 kg/m^3 (Figure 8). Then, the coefficients of diffusion and fixation of alkali were calculated to fit the whole kinetics of the

456 expansion of the two mortars $M_{S50\text{-}L50}$ - 6.2 kg/m^3 and $M_{S17\text{-}L83}$ - 13.4 kg/m^3 (Figure 8). The
457 values thus determined are given in Table 2.

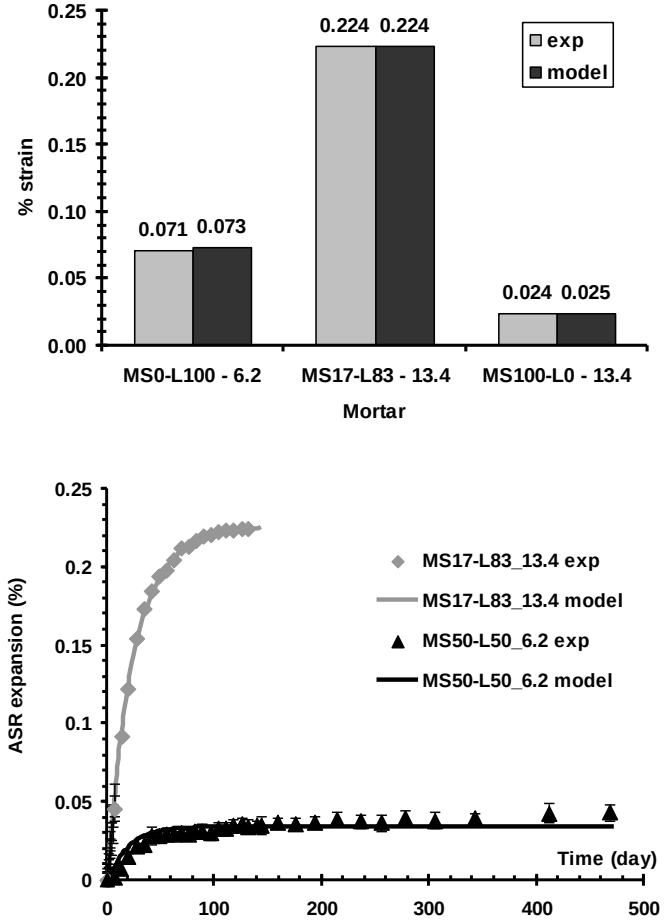

Figure 8 – Identification of chemical parameters on mortars $M_{S0\text{-}L100}$-6.2kg/m^3, $M_{S50\text{-}L50}$-6.2kg/m^3, $M_{S17\text{-}L83}$-13.4kg/m^3 and $M_{S100\text{-}L0}$-13.4kg/m^3

458

459 ## *5.3 Discussion*

460 ### 5.3.1 Curve fitting

461 As shown in Figure 8, the determination of the five parameters of the physicochemical
462 modeling allowed a good representation of ASR expansions to be obtained for two different
463 reactive particle sizes and two different alkali contents. As already observed in the analysis of
464 the experiment [38], the larger the aggregate, the higher the ASR-expansion. The model

explains the decrease of the expansion with the increase in the reactive particle sizes by the movement of a part of the gel into the connected porous zone. The decrease of 90% observed between the small fraction FS and the large fraction FL can be obtained by a thickness of the connected porous zone of about 0.6 µm. The second main parameter of the final expansions of the mortars in the model is the molar volume of ASR gels. The molar volume determined by curve fitting for this experiment, $18.2.10^{-6}$ m^3/mol, is in good agreement with the experimental values obtained on synthetic gels. In [42], the molar volume of synthetic gels similar to natural ASR gels in solution was measured to be between $17.35.10^{-6}$ and $23.65.10^{-6}$ m^3/mol depending on the composition of the gels. The two last parameters have large effects on the kinetics and on the expansion of mortar with low alkali content. Good representation of the expansion curves was obtained with the values given in Table 2.

The threshold of alkali above which the ASR-expansion occurred was assessed by curve fitting. With this threshold and all the parameters given in Table 2, for a mortar with a mean porosity of 18%, ASR expansion occurs for alkali content higher than 4 kg of alkali /m^3 of concrete. This is in good agreement with the usual values given by the literature (3 and 5 kg/m^3) [23-26].

5.3.2 Prediction of other expansions

Once the curve fitting had been performed, all the other expansions were calculated without any additional fitting (Figure 9).

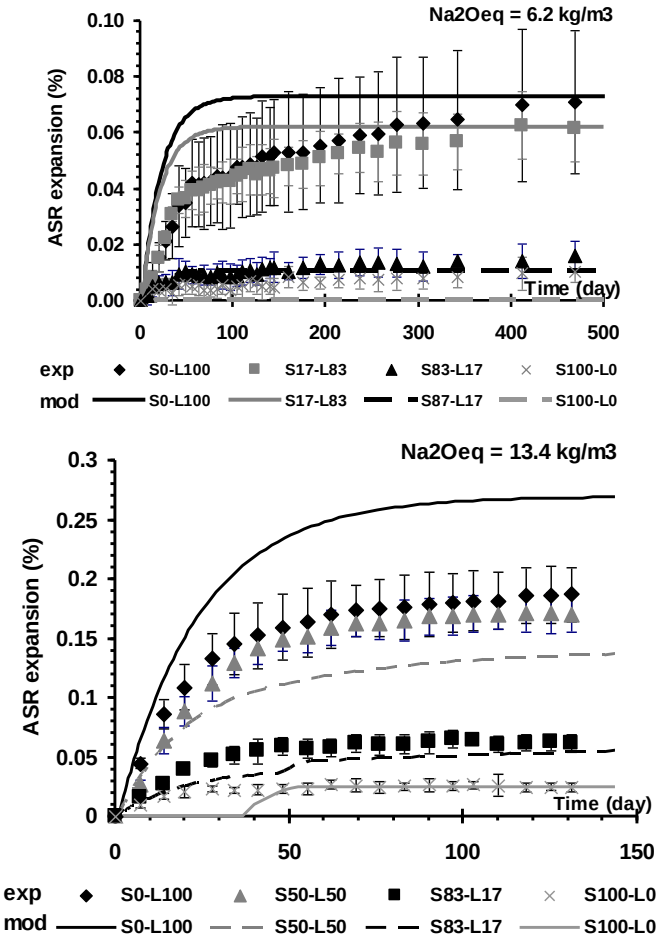

Figure 9 – Prediction of the ASR-expansion of the mortars $M_{S0\text{-}L100}$, $M_{S17\text{-}L83}$, $M_{S83\text{-}L17}$, $M_{S100\text{-}L0}$-6.2kg/m^3 and $M_{S0\text{-}L100}$, $M_{S50\text{-}L50}$, $M_{S83\text{-}L17}$, $M_{S100\text{-}L0}$-13.4kg/m^3

484

485 For the low alkali content, the kinetics appears to be overestimated but the final expansions
486 are well predicted. For the high alkali content, the mortars $M_{S50\text{-}L50}$ and $M_{S83\text{-}L17}$ are quite
487 well-estimated but the prediction of the mortar $M_{S0\text{-}L100}$ is not good. The differences between
488 the calculations and the measurements of the mortar $M_{S50\text{-}L50}$ can be explained by the
489 sensitivity of the model to the porosity of the cement paste. If the same porosity is taken for
490 the mortar $M_{S100\text{-}L0}$ used in the curve fitting and for the mortar $M_{S50\text{-}L50}$, the prediction is
491 perfect for the two mortars. A variation of 1.5% of porosity (it is the difference between the
492 two mortars of the high alkali content $M_{S50\text{-}L50}$ and $M_{S100\text{-}L0}$) gives a variation of about 0.03%
493 in the calculated expansions. The scatter (the porosity of $M_{S0\text{-}L100}$ lies between 19.5% and
494 20.7%) and the high value of porosity (about 20% for $M_{S0\text{-}L100}$, $M_{S17\text{-}L83}$ and $M_{S50\text{-}L50}$ with the

high alkali content) can be responsible for the difficulties experienced in obtaining better agreement for the two mortars $M_{S0\text{-}L100}$ and $M_{S50\text{-}L50}$. The delay observed for the mortar $M_{S100\text{-}L0}$ can be partly explained by the discretization of the particle sizes: in the present study only one average size was used for each aggregate size range (S,M or L). A better description of the size distribution of the finest particles could improve the modeling results.

5.3.3 Interest and limitations of the model

The model presented here is mainly based on a previous model developed by Poyet *et al.* [18]. Several improvements can be noted. In this new model, some considerations have been modified:

- Due to the large difference in the diffusion coefficients of the aggregate and the cement paste, the concentration of alkali in the paste has been considered as homogeneous and is represented by a single variable (no more discretization of the paste around each aggregate like in [18]). The calculated values remain reliable, but the duration of calculation is largely reduced.
- In order to predict the difference of expansion, the mechanical part of the model presents in [18] was partly based on a parameter which depends on the size of the aggregates. Thus, it was not an intrinsic parameter of the material. In the new model, all the mechanical parameters are intrinsic, i.e. independent of the aggregate size. The expansions of aggregate of different size can be deduced without supplementary fitting.
- The definition of a threshold in alkali concentration allows the expansions of mortars containing different alkali contents to be calculated with a good accuracy. No previous models in the literature were tested on this point.

Contrary to the previous model [18], the improved new model presented in this paper allows the prediction of ASR expansions of mortars containing particles of different sizes.

However, the present model still has some limitations. One of the main difficulties in using the model presented above is the determination of the reactive silica content in the aggregate. A method was proposed in [38] for the siliceous limestone studied here, but improvements are still required, particularly to be used for other types of reactive aggregates.

Some papers have shown the replacement of the alkali by calcium in the ASR gels [8-10]. This phenomenon has little effect on the expansion obtained in the laboratory for short periods or for mortars with high alkali content because it appears to occur after long period of exposure. However, it can have important effects on the final expansion in real structures because, once free again, alkali can attack more reactive silica and new expansions are possible [6-7]. Therefore, it will be the next improvement made to the model.

Moreover, the model was developed with several assumptions (about the diffusion, the composition of the ASR gel, the mechanical properties of mortar under long-term loading, etc.). Supplementary investigations are needed before it can be applied to real structures. In particular, the effect of temperature on all the physiochemical and mechanical mechanisms needs to be analyzed (expansion measurements of mortars kept at several temperatures are currently in progress). This paper has shown the effect of the aggregate size on the prediction of the concrete expansion. It should be taken into account in the expert assessments of real structures already performed in [6-7]. Thus, it would be important to study the effects of the discretization of the aggregate size distribution on the expansion predicted.

6. Conclusion

This paper presents an improved empirical microscopic model of ASR expansions based on previous models. It proposes some improvements to take the fixation of alkali into account and to calculate the ASR expansion by means of a mechanical damage variable. The diffusion and the fixation of the alkali are assessed with the mass balance equation. A threshold alkali concentration, above which the formation of the gel starts, is defined; the speed of alkali fixation is assumed to be proportional to the difference between the alkali concentration in the aggregate and this threshold. The mechanical modeling uses a damage variable in order to determine the ASR expansion due to the volume of gel produced by the reaction and determined by the physicochemical part of the model. No parameter of the mechanical model needs fitting. Previous experimental research has been used to check the capability of the model. Four parameters of the physicochemical modeling were determined by curve fitting the expansion curves of four mortars of this experiment. These model parameters have a physical meaning and have been found to be close to previous measurements reported in the literature. The model can reproduce the decrease of expansion with the size of the aggregate, and the increase of expansion with the alkali content. The model is also able to predict the expansions of six other mortars containing two sizes of aggregate and cast with two alkali contents. These calculations have shown the sensitivity of the model to the mortar porosity. Finally, the academic interest of the model lies in the fact that the significance of every assumed mechanism is explained and quantified.

Real structures containing large reactive aggregate (size about 100 mm) are currently being analyzed in the LMDC by using the same assumptions as in this model. In this approach, the largest aggregates are crushed and used to make new mortars with high alkali contents in order to quantify the reactive silica remaining in affected concrete aggregate as rapidly as

564 possible [7]. Kinetics parameters are assessed on these mortars and the model is used to
565 predict the expansion of larger aggregates with different alkali contents. Thus, the model
566 could be used to predict the slow expansion of concrete in structures from the fast expansion
567 of mortar observed in the laboratory.

568 # 7. References

569 [1] P. Léger, P. Cote, R. Tinawi, Finite element analysis of concrete swelling due to Alkali-
570 Aggregate Reaction in Dams, Comput. Struct. 60 (1996) 601-611.
571 [2] S. Malla, M. Wieland, Analysis of an arch-gravity dam with a horizontal crack,
572 Comput. Struct. 72 (1999) 267-278.
573 [3] F. Ulm, O. Coussy, L. Kefei, C. Larive, Thermo-chemo-mechanics of ASR expansion
574 in concrete structures, ASCE J. Eng. Mech. 126 (3) (2000) 233–242.
575 [4] K. Li, O. Coussy, Concrete ASR degradation: from material modeling to structure
576 assessment, Conc. Sc. Eng. 4 (2002) 35-46.
577 [5] V. Saouma, L. Perotti, T. Shimpo, Stress Analysis of Concrete Structures Subjected to
578 Alkali-Aggregate Reactions, ACI Struct. J. 104 (5) (2007) 532-541.
579 [6] E. Grimal, Caractérisation des effets du gonflement provoqué par la réaction alcali-
580 silice sur le comportement mécanique d'une structure en béton, PhD thesis, Université Paul
581 Sabatier Toulouse, France (2007).
582 [7] A. Sellier, E. Bourdarot, S. Multon, M. Cyr, E. Grimal, Assessment of the residual
583 expansion for expertise of structures affected by AAR, 13th Int. Conf AAR, Trondheim,
584 Norway, (2008).
585 [8] J. Duchesne, M-A. Bérubé, Discussion of the Paper "The effectiveness of
586 supplementary cementing materials in suppressing expansion due to ASR – Part 1, Concrete
587 expansion and portlandite depletion", Cem. Conc. Res. 24 (8) (1994) 1572-1573.
588 [9] B. Lagerblad, J. Trägardh, Slowly reacting aggregates in Sweden – Mechanism and
589 conditions for reactivity in concrete, 9th ICAAR, Concrete Society Publication CS 106,
590 London, Great-Britain (1992) 570-578.
591 [10] W.J. French, Maintenance of mobile alkali concentration in cement paste during alkali-
592 aggregate reaction, Enclosure to Proc. 8th ICAAR, Kyoto, Japan (1989).
593 [11] P. Goltermann, Mechanical predictions on concrete deterioration. part 1: Eigenstresses
594 in concrete, ACI Mat. J. 91 (6) (1994) 543–550.

595 [12] Z.P. Bazant, G. Zi, C. Meyer, Fracture mechanics of AAR in concretes with waste glass
596 particles of different sizes, ASCE J. Eng. Mech. 126 (3) (2000) 226–232.
597 [13] Y. Furusawa, H. Ohga, T. Uomoto, An analytical study concerning prediction of
598 concrete expansion due to alkali-silica reaction, in Malhotra (ed.), 3rd Int. Conf. on Durability
599 of Concrete, Nice, France (1994) 757–780. SP 145-40.
600 [14] A. Nielsen, F. Gottfredsen, F. Thogersen, 1993, Development of stresses in concrete
601 structures with alkali-silica reactions, Mater. Struct. 26 (1993) 152-158.
602 [15] A. Sellier, J-P. Bournazel, A. Mébarki, Modelling the alkali aggregate reaction within a
603 probabilistic frame-work, 10th ICAAR, Melbourne, Australia, (1996) 694-701.
604 [16] Z.P Bazant, A. Steffens, Mathematical model for kinetics of alkali-silica reaction in
605 concrete, Cem. Conc. Res. 30 (2000) 419–428.
606 [17] A. Suwito, W. Jin, Y. Xi, C. Meyer, A mathematical model for the pessimum effect of
607 ASR in concrete, Conc. Sc. Eng. 4 (2002) 23-34.
608 [18] S. Poyet, A. Sellier, B. Capra, G. Foray, J.-M. Torrenti, H. Cognon, E. Bourdarot,
609 Chemical modelling of Alkali Silica reaction: Influence of the reactive aggregate size
610 distribution, Mater. Struct., 40 (2007) 229–239.
611 [19] L.S. Dent Glasser, N. Kataoka, The chemistry of Alkali-Aggregate Reactions, 5th
612 ICAAR, Cape Town, South Africa (1981) S252/23.
613 [20] S. Chatterji, 1979, The role of Ca(OH)2 in the breakdown of portland cement concrete
614 due to Alkali-Silica Reaction, Cem. Conc. Res. 9 (1979) 185-188.
615 [21] S. Diamond, ASR – Another look at mechanisms, 8th ICAAR, Kyoto, Japan (1989) 83-
616 94.
617 [22] T.N. Jones, A new interpretation of alkali-silica reaction and expansion mechanisms in
618 concrete, Chemistry and Industry 18 (1988) 40-44.
619 [23] C.A. Rogers, R.D. Hooton, Reduction in mortar and concrete expansion with reactive
620 aggregates due to alkali leaching, Cement, Concrete and Aggregates 13 (1) (1991) 42–49.
621 [24] D.W. Hobbs, Deleterious alkali–silica reactivity in the laboratory and under field
622 conditions, Mag. Conc. Res. 45 (163) (1993) 103–112.
623 [25] M.D.A. Thomas, B.Q. Blackwell, P.J. Nixon, Estimating the alkali contribution from fly
624 ash to expansion due to alkali-aggregate reaction in concrete, Mag. Conc. Res. 48 (177)
625 (1996) 251–264.
626 [26] M.H. Shehata, M.D.A. Thomas, The effect of fly ash composition on the expansion of
627 concrete due to alkali–silica reaction, Cem. Conc. Res. 30 (7) (2000) 1063–1072.

628 [27] S. Diamond, Alkali reactions in concrete – pore solution effects, 6th International
629 Conference on AAR in Concrete, Copenhagen, Denmark (1983) 155-166.
630 [28] P. Rivard, M.A. Bérubé, J-P. Ollivier, G. Ballivy, Decrease of pore solution alkalinity in
631 concrete tested for alkali-silica reaction, Mater. Struc 40 (2007) 909-921.
632 [29] S. Urhan, Alkali Silica and Pozzolanic Reactions in concrete. Part 1 : interpretation of
633 published results and an hypothesis concerning the mechanism, Cem. Conc. Res. 17 (1)
634 (1987) 141-152.
635 [30] N. Thaulow, U-H. Jakobsen, B. Clark, Composition of alkali silica gel and ettringite in
636 concrete railroad ties: SEM-EDX and X-ray diffraction analyses, Cem. Conc. Res. 26 (1996)
637 309-318.
638 [31] H.F.W. Taylor, Cement Chemistry, Academic Press, London, 1990.
639 [32] M. Kawamura, H. Fuwa, Effects of lithium salts on ASR gel composition and expansion
640 of mortars, Cem. Conc. Res. 33 (2003) 919-919.
641 [33] E. Grimal, A. Sellier, Y. Le Pape, E. Bourdarot, Creep shrinkage and anisotropic
642 damage in AAR swelling mechanism, part I: a constitutive model, ACI Mat. J. 105 (3) (2008)
643 227-235.
644 [34] BAEL "Règles techniques de conception et de calcul d'ouvrages et constructions en
645 béton armé suivant la méthode des états limites", Fascicule 62 of CCTG, French design code,
646 1991, modified in 1999.
647 [35] L.M. Kachanov, Introduction to continuum damage mechanics, Martinus Nijhoff
648 Publishers, 1986.
649 [36] J. Lemaître, J.-L. Chaboche, Mécanique des Matériaux Solides, Dunod (Eds.), Paris,
650 France, 1988.
651 [37] T. Siemes, J. Visser, Low tensile strength in older concrete structures with Alkali-Silica
652 Reaction, 11th ICAAR, Quebec, Canada (2000) 1029-1038.
653 [38] S. Multon, M. Cyr, A. Sellier, N. Leklou, L. Petit, Coupled effects of aggregate size and
654 alkali content on ASR expansion, Cem. Conc. Res., 38 (3) (2008) 350-359.
655 [39] AFPC–AFREM (Association Française Pour la Construction – Association Française de
656 Recherche et Essais sur les Matériaux de construction), Durabilité des bétons. Méthodes
657 recommandées pour la mesure des grandeurs associées à la durabilité. Mesure de la masse
658 volumique apparente et de la porosité accessible à l'eau. Compte-Rendu des Journées
659 Techniques, Toulouse, 11-12 Décembre 1997, pp.121–124.
660 [40] S. Poyet, Etude de la dégradation des ouvrages en béton atteints de la réaction alcali-
661 silice: approche expérimentale et modélisation numérique multi-échelle des dégradations dans

un environnement hydrochemo-mécanique variable, PhD thesis, Université de Marne la Vallée, France (2003).

[41] C. Larive, Apports combinés de l'expérimentation et de la modélisation à la compréhension de l'alcali-réaction et de ses effets mécaniques, Laboratoire Central des Ponts et Chaussées (Edt.), Ouvrage d'Art, Rapport OA 28, 1998.

[42] A. Perruchot, P. Massard, J. Lombardi, Composition et volume molaire apparent des gels Ca–Si, une approche expérimentale, C. R. Geoscience 335 (2003) 951–958.

Acknowledgments

The authors are grateful to Electricité De France for supporting this work.

Notations

a	sub or superscript relative to the size fraction of the reactive aggregate
C_{agg}	volume fraction of all the aggregate per m^3 of concrete
C_{Na}	concentration of alkali
C_{Na}^{cp}	alkali concentration in the cement paste
CZ	subscript relative to the cracked zone surrounding the reactive aggregate
D	coefficient of diffusion of alkalis into the aggregate
d	damaged variable
$\underline{\underline{\varepsilon}}$	strain matrix for each material
ε_a	expansion induced by ASR in the aggregate a
ε_{ASR}	total expansion of the concrete
ε_{imp1}	imposed strain applied to the aggregate
ε_{imp2}	imposed strain applied to the cracked zone
E	Young's modulus
E_d	damaged Young's modulus
ϕ_a	volume fraction of reactive aggregates with mean radius R_a
f	coefficient of fixation of alkali
f_t	tensile strength of the mortar
$\underline{\underline{I}}$	unit matrix
M_{Na2O}	mass of equivalent alkali per m^3 of concrete
M^{mol}_{Na2O}	molar mass of equivalent alkali (equal to 0.062 kg/mol)

693 ν Poisson's coefficient of the medium

694 N_a number of reactive aggregate *a* in the final REV

695 Na_{th} alkali threshold above which the attack of reactive silica starts

696 $n_g{}^a$ number of moles of ASR-gel produced by the aggregate *a*

697 p_{agg} porosity of the aggregate

698 p_{cp} porosity of the cement paste

699 p_{mort} porosity of the mortar

700 R_a mean radius of the reactive aggregate of size fraction *a*

701 $R^a{}_{REV}$ REV radius corresponding to the aggregate size fraction *a*

702 $\underline{\underline{\sigma}}$ stress matrix for each material

703 $S(C_{Na})$ depletion term which represents the alkali consumption

704 SC subscript relative to the concrete surrounding the reactive aggregate

705 S_r saturation degree

706 t_c thickness of the connected porous volume filled by the gel

707 u displacement

708 V_g total volume of ASR gel produced

709 $V_{gel}{}^{mol}$ molar volume of the gel

710 V_{po} volume of porosity filled by the gel

711 $\langle X \rangle^+$ equal to X if $X > 0$ or equal to 0 if $X \leq 0$

712